Nonlinear Analysis: Modelling and Control, Vol. 20, No. 4, 603–620 ISSN 1392-5113
http://dx.doi.org/10.15388/NA.2015.4.10

Computational modeling of the bacterial self-organization in a rounded container: the effect of dimensionality*

Romas Baronas[a], **Žilvinas Ledas**[a], **Remigijus Šimkus**[b]

[a]Faculty of Mathematics and Informatics, Vilnius University
Naugarduko str. 24, LT-03225 Vilnius, Lithuania
romas.baronas@mif.vu.lt; zilvinas.ledas@dict.lt

[b]Institute of Biochemistry, Vilnius University
Mokslininkų str. 12, LT-08662 Vilnius, Lithuania
remigijus.simkus@bchi.vu.lt

Received: April 10, 2015 / **Revised:** July 11, 2015 / **Published online:** September 24, 2015

Abstract. A bacterial self-organization in a rounded container as detected by bioluminescence imaging is mathematically modeled by applying the the Keller–Segel approach with logistic growth. The pattern formation in a colony of luminous *Escherichia coli* is numerically simulated by the nonlinear reaction-advection-diffusion equations. In this work, the pattern formation is studied in 3D and the results are compared with previous and new 2D and 1D simulations. The numerical simulation at transition conditions was carried out using the finite difference technique. The simulation results showed that the developed 3D model captures fairly well the sophisticated patterns observed in the experiments. Since the numerical simulation based on the 3D model is very time-consuming, the reduction of spatial dimension of the model for simulating 1D spatiotemporal patterns is discussed. Due to the accumulation of luminous cells near the top three-phase contact line the experimental patterns of the bioluminescence can be qualitatively described by 1D and 2D models by adjusting values of the diffusion coefficient and/or chemotactic sensitivity.

Keywords: chemotaxis, reaction-diffusion, pattern formation, mathematical modelling.

1 Introduction

Bacterial growth and movement in confined suspensions often results in the emergence of millimeter-scale patterns, mainly near the contact lines and surfaces [4, 5, 6, 34, 39]. The interaction of several active processes in the living suspensions leads to very complex dynamic systems which are still poorly understood [7, 41].

Chemotaxis, as the direct movement of cells along the gradient of certain chemicals in their environment, is one of the main phenomenon determining the pattern formation [11]. A vast amount of research, both experimental and theoretical, has been devoted to understanding the chemotaxis, and the analysis of pattern formation in chemotactic systems is

*This work was supported by the Research Council of Lithuania (LMT grant No. MIP-001/2014).

in full swing [7, 14]. Since the pioneering work by Keller and Segel [21] mathematical modeling plays a crucial role in understanding the mechanism of chemotaxis [13]. Quite a number of mathematical models based on reaction-advection-diffusion equations has been developed for modeling the pattern formation in bacterial colonies [7, 9, 20, 23, 27, 28, 29, 33, 36, 44]. However, the system introduced by Keller and Segel remains among the most widely used [8, 10, 13, 16, 22, 25, 26].

According to the Keller and Segel approach, the dynamics of the bacteria, chemoattractant and nutrient (stimulant) are modeled mathematically and give rise to a system of nonlinear partial differential equations [6, 21]. Assuming that the liquid medium contains sufficient nutrient for the cells (or organism), two governing equations are mostly used to describe the dynamics of the cell density and concentration of the chemical signal (chemoattractant) under quasi-steady-state assumption [14, 26, 35, 37]. The growth and death of cells is often ignored assuming the short time course of liquid experiments [13, 16, 36].

The process of the bacterial self-organization is usually observed from different point of view [12]. Colonial patterns of *E. coli* on semi-solid agar surfaces has been studied extensively by microbiologists and physicists [44]. A quasi two-dimensional suspension of the swimming bacteria in a thin chamber of water has been studied experimentally and numerically [8, 15]. The dynamics of *E. coli* cultures was investigated by capturing bioluminescence images observed in circular polystyrene microtiter plate wells and glass containers [39, 42]. In most cases, the investigations are restricted to one (1D) or two (2D) dimensions in space, where only stripes and spots are concerned. Recently, three-dimensional (3D) aggregation patterns based on the volume-filling Keller–Segel model have been studied numerically, and new patterns called P-surfaces, perforated lamellar, completely specific to 3D have been obtained [31]. The 3D simulation was also applied to investigate the activity-induced phase separation in concentrated suspensions of active particles, and important differences between the 2D and 3D cases were found [32].

Computational modeling was also applied to investigate the bacterial self-organization in small rounded containers near the three-phase contact line as detected by quasi-one-dimensional bioluminescence imaging [2, 40]. The spatiotemporal patterns in the fluid cultures of luminous *E. coli* were numerically simulated on the basis of a 1D mathematical model of chemotaxis taking into consideration the cell growth and death. Then, the mathematical model was extended to a 2D model for simulating the bacterial self-organization on the inner top surface as well as on the inner lateral surface of a circular glass test-tube [3, 41]. Although the dynamics of the nutrient (succinate) is often ignored when modeling the bacterial self-organization [10,13,26,35], the simulation of the pattern formation of the cultures of luminous *E. coli* near the lateral surface showed that the dynamics of the nutrient (oxygen) should be considered in addition to the bacteria and chemoattractant [41].

The aim of this work was to generalize the known mathematical models of the bacterial self-organization to a 3D model to be used for simulating spatiotemporal patterns in the fluid cultures of luminous *E. coli* in a rounded container. The numerical simulation at the transient conditions was carried out using the finite difference technique [30]. The mathematical model and the numerical solution were validated by experimental data [39,

42]. The numerical simulation showed that the developed model captures fairly well the sophisticated patterns observed in the experiments.

Since the simulation based on 3D model is very time-consuming, therefore reducing spatial dimensionality in a model for simulating 1D and 2D spatiotemporal patterns was investigated. The patterns simulated by models of different dimensionality were compared with each other and with the experimental patterns. Due to the accumulation of luminous cells near the top three-phase contact line the experimental patterns of the bioluminescence were qualitatively simulated using 1D and 2D models by adjusting values of the diffusion coefficient and/or chemotactic sensitivity.

2 Mathematical modeling

We model the spatiotemporal pattern formation in the fluid cultures of luminous *E. coli* placed in a rounded glass container. Assuming the direct proportionality between the bioluminescence and the number of active cells the bacterial self-organization can be modeled by the dynamics of the density of bioluminescent cells [40].

The container is modeled by a right circular cylinder. Figure 1 shows the principal structure of the rounded container, where r and h are the base radius and the height of the cylinder, respectively. For simplicity, it was assumed that the fluid fills the container.

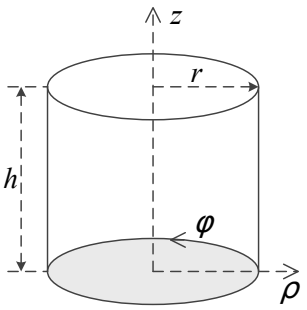

Fig. 1. Principal structure of the rounded container.

2.1 Governing equations

Translating the main biological processes into a mathematical model leads to a system of three conservation equations [6, 35, 37]

$$\begin{aligned}
\frac{\partial n}{\partial t} &= D_n \Delta n - \nabla\big(f_s(n,c) n \nabla c\big) + f_g(n,s),\\
\frac{\partial c}{\partial t} &= D_c \Delta c + g_p(n,c) n - g_d(n,c) c,\\
\frac{\partial s}{\partial t} &= D_s \Delta s - h(n,s), \quad \mathrm{x} \in \Omega \subset \mathbb{R}^n,\ t > 0,
\end{aligned} \tag{1}$$

where Δ is the Laplace operator, x and t stand for space and time, $n(\mathrm{x}, t)$ denotes the cell density, $c(\mathrm{x}, t)$ is the chemoattractant concentration, $s(\mathrm{x}, t)$ is the concentration of a nutrient (succinate, stimulant), D_n, D_c and D_s are the diffusion coefficients usually assumed to be constant, $f_g(n, s)$ stands for cell growth and death, $f_s(n, c)$ denotes the chemotactic sensitivity, g_p and g_d stand for the production and degradation of the chemoattractant, respectively, and $h(n, s)$ stands for the nutrient consumption.

Recently, it was shown that the sensitivity of cells to attractant can be successfully assumed to be independent of the chemoattractant concentration when modeling the bacterial self-organization in a rounded container along the contact line as detected by bioluminescence imaging [2], i.e. $f_s(n, c)$ can be constant, $f_s(n, c) = k_1$.

The cell growth is usually assumed to be logistic, i.e. $f_g(n, c) = k_2 n(1 - n/k)$, where k_2 is the growth rate of the cell population, and k is the cell density under steady-state conditions or the carrying capacity [10, 13, 14, 26, 27]. Although k_2 and k are often assumed to be constant, in this work we assume a more general case by modeling k as a linear function of the nutrient concentration, i.e. $k = k_3 s$. The linear dependence between carrying capacity and limited resources was also explored, for example, in certain population growth models [17, 19].

A number of chemoattractant production functions have been used in chemotactic models [13]. Usually, a saturating function of the cell density is used indicating that, as the cell density increases, the chemoattractant production decreases. The Michaelis–Menten function is widely used to express the chemoattractant production, $g_p(n, c) = k_4/(k_5 + n)$ [21, 23, 25]. The degradation or consumption of the chemoattractant is typically linear, $g_d(n, c) = k_6$, where k_6 is a constant [13].

Consumption $h(n, s)$ of the nutrient was assumed to be directly proportional to the population density, $h(n, s) = k_7 n$. Similar approach was used in investigating the rate of dissolved oxygen consumption by different viable cells in a bioreactor [18], as well as in certain population growth models [17, 19].

Inserting the concrete expressions of f_s, f_g, g_p, g_d and h to system (1) leads to the following governing equations of the population kinetics model:

$$\begin{aligned}
\frac{\partial n}{\partial t} &= D_n \Delta n - \nabla(k_1 n \nabla c) + k_2 n\left(1 - \frac{n}{k_3 s}\right), \\
\frac{\partial c}{\partial t} &= D_c \Delta c + \frac{k_4 n}{k_5 + n} - k_6 c, \\
\frac{\partial s}{\partial t} &= D_s \Delta s - k_7 n, \quad \mathrm{x} \in \Omega,\ t > 0,
\end{aligned} \tag{2}$$

where k_1 is the chemotactic sensitivity, k_2 is the growth rate of the cell population, k_3 stands for the cell density under steady-state conditions, k_4 and k_5 stand for saturating chemoattractant production, k_6 and k_7 are the consumption rates of the chemoattractant and the nutrient, respectively, the other notations are the same as in model (1). All the parameters are assumed to be constant and positive.

Assuming the rounded container as a right circular cylinder, the mathematical model of the bacterial self-organization in the container (domain Ω) can be defined in cylindrical

coordinates,

$$\begin{aligned} &\mathrm{x} = (\rho, \varphi, z), \\ &\Omega = (0, r) \times (0, 2\pi) \times (0, h), \\ &\Delta F = \frac{1}{\rho}\frac{\partial}{\partial \rho}\left(\rho \frac{\partial F}{\partial \rho}\right) + \frac{1}{\rho^2}\frac{\partial^2 F}{\partial \varphi^2} + \frac{\partial^2 F}{\partial z^2}, \end{aligned} \tag{3}$$

where r and h are the base radius and the height of the cylinder Ω as shown in Fig. 1.

2.2 Initial and boundary conditions

We assume a possibly non-uniform initial (at $t = 0$) distribution of cells, chemoattractant and nutrient,

$$\begin{aligned} &n(\rho, \varphi, z, 0) = n_{0\mathrm{x}}(\rho, \varphi, z), \quad c(\rho, \varphi, z, 0) = c_{0\mathrm{x}}(\rho, \varphi, z), \\ &s(\rho, \varphi, z, 0) = s_{0\mathrm{x}}(\rho, \varphi, z), \quad (\rho, \varphi, z) \in [0, r] \times [0, 2\pi) \times [0, h], \end{aligned} \tag{4}$$

where $n_{0\mathrm{x}}(\rho, \varphi, z)$, $c_{0\mathrm{x}}(\rho, \varphi, z)$ and $s_{0\mathrm{x}}(\rho, \varphi, z)$ stand for the initial ($t = 0$) cell density, chemoattractant and nutrient concentrations, respectively.

The no-leak boundary conditions ($t > 0$) are applied on the base of the glass vessel,

$$D_n \frac{\partial n}{\partial z}\bigg|_{z=0} = 0, \quad D_c \frac{\partial c}{\partial z}\bigg|_{z=0} = 0, \quad D_s \frac{\partial s}{\partial z}\bigg|_{z=0} = 0, \quad (\rho, \varphi) \in [0, r] \times [0, 2\pi). \tag{5}$$

At the top surface the fluid contacts with the atmosphere containing a nutrient, e.g. oxygen. We assume a constant concentration of nutrient at that surface, while no-leak conditions for the cells as well as for the chemoattractant,

$$D_n \frac{\partial n}{\partial z}\bigg|_{z=h} = 0, \quad D_c \frac{\partial c}{\partial z}\bigg|_{z=h} = 0, \quad s(\rho, \varphi, h, t) = s_0, \quad (\rho, \varphi) \in [0, r] \times [0, 2\pi). \tag{6}$$

Due to the continuity in the azimuth direction of the vessel, the periodicity conditions are used in φ direction ($t > 0$),

$$\begin{aligned} &n(\rho, 0, z, t) = n(\rho, 2\pi, z, t), \quad c(\rho, 0, z, t) = c(\rho, 2\pi, z, t), \\ &s(\rho, 0, z, t) = s(\rho, 2\pi, z, t), \\ &D_n \frac{\partial n}{\partial \varphi}\bigg|_{\varphi=0} = D_n \frac{\partial n}{\partial \varphi}\bigg|_{\varphi=2\pi}, \quad D_c \frac{\partial c}{\partial \varphi}\bigg|_{\varphi=0} = D_c \frac{\partial c}{\partial \varphi}\bigg|_{\varphi=2\pi}, \\ &D_s \frac{\partial s}{\partial \varphi}\bigg|_{\varphi=0} = D_s \frac{\partial s}{\partial \varphi}\bigg|_{\varphi=2\pi}, \quad (\rho, z) \in [0, r] \times [0, h]. \end{aligned} \tag{7}$$

The non-permeability of the lateral surface of the tube leads to the following boundary conditions:

$$\begin{aligned} &D_n \frac{\partial n}{\partial \rho}\bigg|_{\rho=0} = D_n \frac{\partial n}{\partial \rho}\bigg|_{\rho=r} = 0, \quad D_c \frac{\partial c}{\partial \rho}\bigg|_{\rho=0} = D_c \frac{\partial c}{\partial \rho}\bigg|_{\rho=r} = 0, \\ &D_s \frac{\partial s}{\partial \rho}\bigg|_{\rho=0} = D_s \frac{\partial s}{\partial \rho}\bigg|_{\rho=r} = 0, \quad (\varphi, z) \in [0, 2\pi) \times [0, h]. \end{aligned} \tag{8}$$

2.3 Dimensionless model

In order to define the main governing parameters of the mathematical model (2), (4)–(8), a dimensionless mathematical model has to be derived [13, 24, 25].

A dimensionless model can be derived by setting

$$
\begin{aligned}
&u = \frac{n}{n_0}, \quad v = \frac{k_5 k_6 c}{k_4 n_0}, \quad w = \frac{k_3 s}{n_0},\\
&t^* = k_6 t, \quad \rho^* = \sqrt{\frac{k_6}{D_c}}\rho, \quad \varphi^* = \varphi, \quad z^* = \sqrt{\frac{k_6}{D_c}}z,\\
&D_u = \frac{D_n}{D_c}, \quad D_w = \frac{D_s}{D_c}, \quad \chi = \frac{k_1 k_4 n_0}{k_5 k_6 D_c}, \quad \alpha = \frac{k_2}{k_6}, \quad \beta = \frac{n_0}{k_5}, \quad \gamma = \frac{k_7 k_3}{k_6},
\end{aligned}
\tag{9}
$$

where n_0 is the cell density under steady state conditions. When modeling the carrying capacity by a linear function of the nutrient concentration ($k_3 s$), the cell density under steady state conditions is directly proportional to the concentration s_0 of the nutrient near the top surface, $n_0 = k_3 s_0$.

Dropping the asterisks, the dimensionless governing equations then become

$$
\begin{aligned}
&\frac{\partial u}{\partial t} = D_u \Delta u - \chi \nabla(u \nabla v) + \alpha u\left(1 - \frac{u}{w}\right),\\
&\frac{\partial v}{\partial t} = \Delta v + \frac{u}{1+\beta u} - v,\\
&\frac{\partial w}{\partial t} = D_w \Delta w - \gamma u, \quad (\rho, \varphi, z) \in (0, R) \times (0, 2\pi) \times (0, H),\ t > 0.
\end{aligned}
\tag{10}
$$

where u is the dimensionless cell density, v is the dimensionless chemoattractant concentration, w is the dimensionless concentration of the nutrient, α is the dimensionless growth rate of the cell population, β stands for saturating of the signal production, γ is dimensionless consumption rate of the nutrient, R and H are the relative radius and height of the cylinder, $R = r\sqrt{k_6/D_c}$, $H = h\sqrt{k_6/D_c}$.

The initial conditions (4) take the following dimensionless form:

$$
\begin{aligned}
&u(\rho, \varphi, z, 0) = u_{0\mathrm{x}}(\rho, \varphi, z), \quad v(\rho, \varphi, z, 0) = v_{0\mathrm{x}}(\rho, \varphi, z),\\
&w(\rho, \varphi, z, 0) = w_{0\mathrm{x}}(\rho, \varphi, z), \quad (\rho, \varphi, z) \in [0, R] \times [0, 2\pi) \times [0, H],
\end{aligned}
\tag{11}
$$

where $u_{0\mathrm{x}}(\rho, \varphi, z) = n_{0\mathrm{x}}(\rho, \varphi, z)/n_0$, $v_{0\mathrm{x}}(\rho, \varphi, z) = k_5 k_6 c_{0\mathrm{x}}(\rho, \varphi, z)/(k_4 n_0)$ and $w_{0\mathrm{x}}(\rho, \varphi, z) = k_3 s_{0\mathrm{x}}(\rho, \varphi, z)/n_0$.

The boundary conditions (5)–(8) transform to the following dimensionless equations ($t > 0$):

$$
\begin{aligned}
&D_u \left.\frac{\partial u}{\partial z}\right|_{z=0} = 0, \quad \left.\frac{\partial v}{\partial z}\right|_{z=0} = 0, \quad D_w \left.\frac{\partial w}{\partial z}\right|_{z=0} = 0,\\
&(\rho, \varphi) \in [0, R] \times [0, 2\pi),
\end{aligned}
\tag{12}
$$

$$
\begin{aligned}
&D_u \left.\frac{\partial u}{\partial z}\right|_{z=H} = 0, \quad \left.\frac{\partial v}{\partial z}\right|_{z=H} = 0, \quad w(\rho, \varphi, H, t) = w_0,\\
&(\rho, \varphi) \in [0, R] \times [0, 2\pi),
\end{aligned}
\tag{13}
$$

$$
\begin{aligned}
&u(\rho,0,z,t)=u(\rho,2\pi,z,t),\quad v(\rho,0,z,t)=v(\rho,2\pi,z,t),\\
&w(\rho,0,z,t)=w(\rho,2\pi,z,t),\\
&D_u\frac{\partial u}{\partial\varphi}\bigg|_{\varphi=0}=D_u\frac{\partial u}{\partial\varphi}\bigg|_{\varphi=2\pi},\quad \frac{\partial v}{\partial\varphi}\bigg|_{\varphi=0}=\frac{\partial v}{\partial\varphi}\bigg|_{\varphi=2\pi},\\
&D_w\frac{\partial w}{\partial\varphi}\bigg|_{\varphi=0}=D_w\frac{\partial w}{\partial\varphi}\bigg|_{\varphi=2\pi},\quad (\rho,z)\in[0,R]\times[0,H],
\end{aligned}
\tag{14}
$$

$$
\begin{aligned}
&D_u\frac{\partial u}{\partial\rho}\bigg|_{\rho=0}=D_u\frac{\partial u}{\partial\rho}\bigg|_{\rho=R}=0,\quad \frac{\partial v}{\partial\rho}\bigg|_{\rho=0}=\frac{\partial v}{\partial\rho}\bigg|_{\rho=R}=0,\\
&D_w\frac{\partial w}{\partial\rho}\bigg|_{\rho=0}=D_w\frac{\partial w}{\partial\rho}\bigg|_{\rho=R}=0,\quad (\varphi,z)\in[0,2\pi)\times[0,H].
\end{aligned}
\tag{15}
$$

2.4 Population dynamics near the top surface

The bacterial self-organization near the inner top surface of a rounded container can be modeled by applying the common 3D mathematical model (2), (4)–(8) as well as the corresponding dimensionless model (10)–(15). However, transient computational simulations based on 3D mathematical models are extremely time and resource consuming. The dimension reduction is a widely used approach for increasing efficiency of the numerical simulation [33].

When modeling the bacterial self-organization near the top surface of a right circular container, the mathematical model can be defined in the polar coordinates on a 2D domain - a circle [3]. Due to a constant concentration of the nutrient near the top surface ($s(\rho,\varphi,h,t)=s_0$ and $w(\rho,\varphi,H,t)=w_0$), the dynamics of the nutrient concentration can be ignored.

Due to modeling the carrying capacity by a linear function of the nutrient concentration ($k_3 s$ in (2)) and the assumption $n_0=k_3 s_0$, the term $k_2 n(1-n/(k_3 s))$ of the logistic cell growth reduces to $k_2 n(1-n/n_0)$, while the corresponding dimensionless term $\alpha u(1-u/w)$ approaches $\alpha u(1-u)$. The dynamics of the bacterial population near the top surface of a right circular container can be described by the following governing equations formulated in polar coordinates:

$$
\begin{aligned}
&\frac{\partial u}{\partial t}=D_u\Delta u-\chi\nabla(u\nabla v)+\alpha u(1-u),\\
&\frac{\partial v}{\partial t}=\Delta v+\frac{u}{1+\beta u}-v,\quad (\rho,\varphi)\in(0,R)\times(0,2\pi),\ t>0,
\end{aligned}
\tag{16}
$$

where Δ is the Laplace operator in the polar coordinates ρ and φ, u and v are functions of two parameters ρ and φ.

The initial conditions (11) take the following form:

$$
u(\rho,\varphi,0)=u_{0\mathrm{x}}(\rho,\varphi),\quad v(\rho,\varphi,0)=v_{0\mathrm{x}}(\rho,\varphi),\quad (\rho,\varphi)\in[0,R]\times[0,2\pi).
\tag{17}
$$

The boundary conditions (12)–(15) reduce to the following equations ($t > 0$):

$$u(\rho,0,t) = u(\rho,2\pi,t), \quad v(\rho,0,t) = v(\rho,2\pi,t),$$
$$D_u \frac{\partial u}{\partial \varphi}\bigg|_{\varphi=0} = D_u \frac{\partial u}{\partial \varphi}\bigg|_{\varphi=2\pi}, \quad \frac{\partial v}{\partial \varphi}\bigg|_{\varphi=0} = \frac{\partial v}{\partial \varphi}\bigg|_{\varphi=2\pi}, \quad \rho \in [0,R], \tag{18}$$

$$D_u \frac{\partial u}{\partial \rho}\bigg|_{\rho=0} = D_u \frac{\partial u}{\partial \rho}\bigg|_{\rho=R} = 0, \quad \frac{\partial v}{\partial \rho}\bigg|_{\rho=0} = \frac{\partial v}{\partial \rho}\bigg|_{\rho=R} = 0, \quad \varphi \in [0,2\pi). \tag{19}$$

2.5 Population dynamics near the three phase contact line

When observing patterns of inhomogeneous bioluminescence in small cylindrical containers made of glass and polystyrene, the bioluminescence images of bacterial cultures showed an accumulation of luminous bacteria near the three-phase contact line [39, 42]. The bacterial self-organization in a circular container along the contact line was mathematically described on a 1D domain – the circumference of the top surface and numerically investigated [2, 40].

The dynamics of the bacterial population near the three phase contact line can be modeled also by applying the common 3D mathematical model (10)–(15) (accepting $\rho = R$, $z = H$) as well as 2D mathematical model (16)–(19) (accepting $\rho = R$). However, the dimension of these model could be reduce to one.

When investigating the population dynamics near the three phase contact line, the radial transport of cells and chemoattractant can be ignored because of the zero flux conditions at the three phase contact line ($\rho = R$ in model (10)–(15)).

The dynamics of the bacterial population near the circumference of the top surface of right circular cylinder can be approximated by the following governing equations formulated in one polar coordinate φ,

$$\begin{aligned} \frac{\partial u}{\partial t} &= D_u \frac{1}{R^2}\frac{\partial^2 u}{\partial \varphi^2} - \chi \frac{1}{R^2}\frac{\partial}{\partial \varphi}\left(u \frac{\partial v}{\partial \varphi}\right) + \alpha u\,(1-u)\,, \\ \frac{\partial v}{\partial t} &= \frac{1}{R^2}\frac{\partial^2 v}{\partial \varphi^2} + \frac{u}{1+\beta u} - v, \quad \varphi \in (0,2\pi),\ t > 0, \end{aligned} \tag{20}$$

where u and v are functions of one parameter φ.

The initial conditions (17) reduce to the following equations:

$$u(\varphi,0) = u_{0\mathrm{x}}(\varphi), \quad v(\varphi,0) = v_{0\mathrm{x}}(\varphi), \quad \varphi \in [0,2\pi). \tag{21}$$

The boundary conditions take the following form ($t > 0$):

$$u(0,t) = u(2\pi,t), \quad v(0,t) = v(2\pi,t),$$
$$D_u \frac{\partial u}{\partial \varphi}\bigg|_{\varphi=0} = D_u \frac{\partial u}{\partial \varphi}\bigg|_{\varphi=2\pi}, \quad \frac{\partial v}{\partial \varphi}\bigg|_{\varphi=0} = \frac{\partial v}{\partial \varphi}\bigg|_{\varphi=2\pi}. \tag{22}$$

When modeling the bacterial self-organization in a quasi-one dimensional ring, using the longitudinal analysis is often more reasonable than the azimuth one [2,40,42]. The 1D mathematical model (20)–(22) can be reformulated by replacing the azimuth parameter φ with the longitudinal parameter x by applying $x = \varphi R$,

$$\begin{aligned} &\frac{\partial u}{\partial t} = D_u \frac{\partial^2 u}{\partial x^2} - \chi \frac{\partial}{\partial x}\left(u \frac{\partial v}{\partial x}\right) + \alpha u(1-u), \\ &\frac{\partial v}{\partial t} = \frac{\partial^2 v}{\partial x^2} + \frac{u}{1+\beta u} - v, \quad x \in (0, L),\ t > 0, \end{aligned} \tag{23}$$

where u and v are functions of one parameter x. L is the dimensionless length of the contact line, i.e. the circumference of the vessel (a circle), $L = 2\pi R = 2\pi r\sqrt{k_6/D_c}$, where r is dimensional radius of the base of the cylinder as shown in Fig. 1.

The initial (21) and the boundary (22) conditions take the following form:

$$u(x,0) = u_{0\mathrm{x}}(x), \quad v(x,0) = v_{0\mathrm{x}}(x), \quad x \in [0, L), \tag{24}$$

$$\begin{aligned} &u(0,t) = u(L,t), \quad v(0,t) = v(L,t), \\ &D_u \left.\frac{\partial u}{\partial x}\right|_{x=0} = D_u \left.\frac{\partial u}{\partial x}\right|_{x=L}, \quad \left.\frac{\partial v}{\partial x}\right|_{x=0} = \left.\frac{\partial v}{\partial x}\right|_{x=L}, \quad t > 0. \end{aligned} \tag{25}$$

The mathematical model (23)–(25) has been successfully used to study the bacterial self-organization of luminous *E. coli* along the contact line of the circular container as detected by bioluminescence imaging [2, 38, 40]. Here this model was derived as a very special case of the common 3D mathematical model (10)–(15).

2.6 Population dynamics near the lateral surface

Recently, the bacterial self-organization in a circular glass test-tube near the inner lateral surface of the vessel was mathematically described in a 2D domain and numerically investigated [41]. Simulated populations of luminous *E. coli* formed bamboo foam-like structures similar to the experimentally observed structures near the inner lateral surface of the vessel [41].

The dynamics of the bacterial population near the lateral surface can be modeled also by applying the common 3D mathematical model (10)–(15) (accepting $\rho = R$). The radial transport of cells u, chemoattractant v and nutrient w can be ignored because of the zero flux condition for u, v and w at the lateral surface ($\rho = R$ in model (10)–(15)).

The dynamics of the bacterial population near the lateral surface of a right circular cylinder can be approximately described by equations (10)–(14) by replacing parameter ρ with a constant R and assuming functions u, v and w as of only two parameters φ and z. Since the lateral surface of a right circular cylinder is a rectangle, the corresponding mathematical model could be defined in the Cartesian coordinates system.

The mathematical model (10)–(14) defined in a 2D domain $[0, 2\pi) \times [0, H]$ can be transformed into a model defined in Cartesian system in a domain $[0, L] \times [0, H]$ by

replacing the azimuth parameter φ with the longitudinal parameter x, $x = R\varphi$ and keeping the height parameter h unchanged.

The bacterial self-organization near the lateral surface can be defined in Cartesian system in the same manner as (10) only adjusting the domain and the Laplace operator,

$$\begin{aligned}
&\frac{\partial u}{\partial t} = D_u\left(\frac{\partial^2 u}{\partial x^2} + \frac{\partial^2 u}{\partial z^2}\right) - \chi\left(\frac{\partial}{\partial x}\left(u\frac{\partial v}{\partial x}\right) + \frac{\partial}{\partial z}\left(u\frac{\partial v}{\partial z}\right)\right) + \alpha u\left(1 - \frac{u}{w}\right),\\
&\frac{\partial v}{\partial t} = \frac{\partial^2 v}{\partial x^2} + \frac{\partial^2 v}{\partial z^2} + \left(\frac{u}{1+\beta u} - v\right),\\
&\frac{\partial w}{\partial t} = D_w\left(\frac{\partial^2 w}{\partial x^2} + \frac{\partial^2 w}{\partial z^2}\right) - \gamma u, \quad (x,z) \in (0,L)\times(0,H),\ t > 0.
\end{aligned} \tag{26}$$

where u, v and w are functions of two parameters x and z, L is the dimensionless circumference of the cylinder base, and H is dimensionless height of the cylinder, $L = 2\pi R = 2\pi r\sqrt{k_6/D_c}$, $H = h\sqrt{k_6/D_c}$.

The initial conditions (11) take the following form ($t = 0$):

$$\begin{aligned}
&u(x,z,0) = u_{0\mathrm{x}}(x,z), \quad v(x,z,0) = v_{0\mathrm{x}}(x,z),\\
&w(x,z,0) = w_{0\mathrm{x}}(x,z), \quad (x,z) \in [0,L]\times[0,H].
\end{aligned} \tag{27}$$

The boundary conditions (12)–(14) transform to the following conditions ($t > 0$):

$$D_u\frac{\partial u}{\partial z}\bigg|_{z=0} = 0, \quad \frac{\partial v}{\partial z}\bigg|_{z=0} = 0, \quad D_w\frac{\partial w}{\partial z}\bigg|_{z=0} = 0, \quad x \in [0,L], \tag{28}$$

$$D_u\frac{\partial u}{\partial z}\bigg|_{z=H} = 0, \quad \frac{\partial v}{\partial z}\bigg|_{z=H} = 0, \quad w(x,H,t) = w_0, \quad x \in [0,L], \tag{29}$$

$$\begin{aligned}
&u(0,z,t) = u(L,z,t), \quad v(0,z,t) = v(L,z,t),\\
&w(0,z,t) = w(L,z,t),\\
&\frac{\partial u}{\partial x}\bigg|_{x=0} = \frac{\partial u}{\partial x}\bigg|_{x=L}, \quad \frac{\partial v}{\partial x}\bigg|_{x=0} = \frac{\partial v}{\partial x}\bigg|_{x=L},\\
&\frac{\partial w}{\partial x}\bigg|_{x=0} = \frac{\partial w}{\partial x}\bigg|_{x=L}, \quad z \in [0,H].
\end{aligned} \tag{30}$$

The 2D mathematical model (26)–(30) has been already applied to investigate the bacterial self-organization of luminous *E. coli* near the lateral surface of the circular test-tube as detected by bioluminescence imaging [41]. Here it was showed that the 2D model (26)–(30) is a special case of the common 3D mathematical model (10)–(15).

3 Numerical simulation

The above described mathematical model as well as corresponding dimensionless models were defined as the initial boundary value problems based on a system of nonlinear partial

differential equations. Because of the nonlinearity of the problem, no exact analytical solutions could be derived in the general case [24,29,37]. Hence the numerical simulation of the bacterial self-organization was used.

There were four special cases analysed: the 3D model (10)–(15); the two-dimensional-in-space of the top surface (2D polar) model (16)–(19); the one-dimensional-in-space of the top contact line (1D) model (23)–(25); and the two-dimensional-in-space of the lateral surface (2D Cartesian) model (26)–(30).

The functions used for the 3D model initial conditions were:

$$\begin{aligned} &u_{0\mathrm{x}}(\rho,\varphi,z) = 1 + 0.2\sin\left(\frac{\varphi * 11}{2}\right)\frac{\rho}{R}, \quad v_{0\mathrm{x}}(\rho,\varphi,z) = 0,\\ &w_{0\mathrm{x}}(\rho,\varphi,z) = 1, \quad (\rho,\varphi,z) \in [0,R]\times[0,2\pi)\times[0,H], \end{aligned} \tag{31}$$

and same were adapted for the 2D and 1D models as well.

The numerical simulations were carried out using the finite difference technique [30]. To find a numerical solution of the problem a uniform discrete grid $40 \times 224 \times 80$ was introduced in space directions and the constant dimensionless step size 0.00005 was also used in the time direction. These values were used for all four cases analysed accordingly for the existing dimensions. The simulations have been checked with a variety of space and time discretizations, and verified that the obtained patterns shown below are almost independent of the space and time steps. An explicit finite difference scheme has been built as a result of the difference approximation [30]. The digital simulator has been programmed by the authors in Free Pascal language.

To simulate spatiotemporal patterns of the quasi-one-dimensional cell density $u_{1\mathrm{D}-2\mathrm{D},\varphi}$ in a vessel near the three-phase contact line by applying the 2D polar model (16)–(19), the density u of cells was integrated over the thin ring close to the outer boundary of the thickness δ and then averaged,

$$u_{1\mathrm{D}-2\mathrm{D},\rho}(\varphi,t) = \frac{2}{1-(1-\delta)^2}\int\limits_{1-\delta}^{1} u(\rho,\varphi,t)\rho\,\mathrm{d}\rho, \quad \varphi\in[0,2\pi],\ t\in[0,T]. \tag{32}$$

Similarly, when applying 2D Cartesian model (26)–(30), the density u of cells was integrated over the whole depth and then averaged,

$$u_{1\mathrm{D}-2\mathrm{D},z}(x,t) = \frac{1}{H}\int\limits_{0}^{H} u(x,z,t)\,\mathrm{d}z, \quad x\in[0,L],\ t\in[0,T]. \tag{33}$$

When applying 3D model (10)–(15), the density u of cells was integrated over the whole depth over the thin ring close to the lateral surface and then averaged,

$$\begin{aligned} &u_{1\mathrm{D}-3\mathrm{D}}(\varphi,t) = \frac{1}{H}\int\limits_{0}^{H}\left(\frac{2}{1-(1-\delta)^2}\int\limits_{1-\delta}^{1} u(\rho,\varphi,z,t)\rho\,\mathrm{d}\rho\right)\mathrm{d}z,\\ &\varphi\in[0,2\pi],\ t\in[0,T]. \end{aligned} \tag{34}$$

4 Results and discussion

Figure 2 shows the spatiotemporal patterns of the quasi-one-dimensional cell density simulated by four versions of the model, while Fig. 3 – a visualization of arbitrary frames of cell density when simulating in 3D at the following values of the model parameters:

$$\begin{aligned} &D_u = 0.1, \quad D_w = 0.2, \quad \chi = 8.3, \quad \alpha = 1, \quad \beta = 0.73, \\ &\gamma = 0.025, \quad R = 5, \quad H = 10, \quad \delta = 0.075, \quad T = 400. \end{aligned} \tag{35}$$

One can see in Fig. 3 that the cell density u inside the rounded container forms foam-like structures similar to the experimentally observed structures [41,42]. In the initial stage of the population evolution, the cells are non-uniformly distributed in entire container, while later the population concentrates near the top surface were the oxygen concentrates.

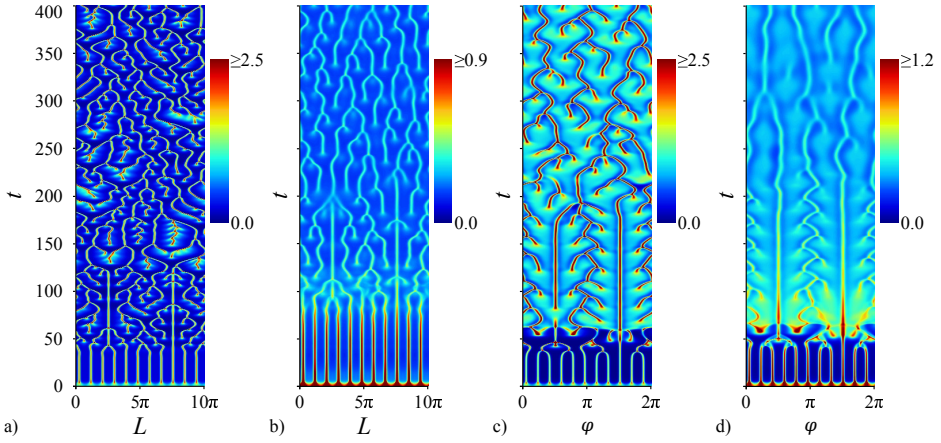

Fig. 2. Spatiotemporal plots of the dimensionless cell density u for four analysed cases: 1D model (a), 2D Cartesian model (b), 2D polar model (c) and 3D model (d). Values of the parameters are as defined in (35).

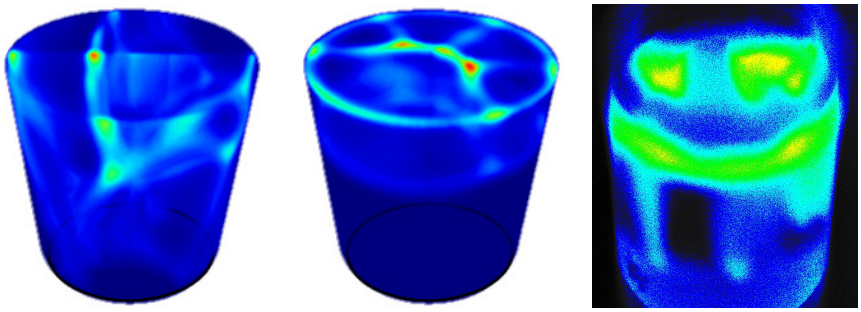

Fig. 3. Visualization of arbitrary frames at u concentrations obtained by 3D simulation at two time moments: 65 and 329. The snapshot of the experimental culture is shown for comparison.

The simulation results also shows (Fig. 2) that the basic spatiotemporal patterns are preserved when reducing the model dimension: merging and emerging dynamics are present in all four simulations of the pattern formation near the three-phase contact line. On the other hand, the simulated spatiotemporal patterns are not very similar among themselves, though values of the model parameters were the same. The patterns obtained by using 2D (Figs. 2b and 2c) and 3D (Fig. 2d) look more similar to those observed experimentally [40, 41, 42] than that obtained by 1D simulation (Fig. 2a). When reducing the dimension (Fig. 2d to 2bc to 2a) the average number of formations (peaks in density) along the contact line tends to increase.

From Fig. 2c and 2d it can be seen that in the initial stage of the population evolution while oxygen (w) is available in the entire container and is not consumed yet, the population simulated by 3D model behaves similarly to that simulated by 2D polar model yet this similarity depends on initial conditions [2, 38].

The difference in the simulated spatiotemporal patterns (Fig. 2) could be explained by assumptions used for reduction of the dimensionality, a relatively large domain size and the sensitivity to the initial conditions. Distinct initial conditions lead not only to distinct pattern types, but certain initial conditions may evolve even to a steady state, while others lead to periodic patterns of varying period [14]. As the domain size is increased, more and more modes become unstable [26], and this corresponds to an increase in the dimension of the attractor, and supports higher levels of complexity [1]. In three dimensions for small growth rate α and constant w, the governing equations (10) may actually generate even unbounded solutions [43]. Using 3D model also permits producing very specific patterns, such as P-surface, which never exist in lower dimensions [31]. Important differences between the physics of the 2D and 3D systems were also found when investigating the activity-induced phase separation in concentrated suspensions of active particles, for instance, the shape of the phase diagram and the region within which phase separation was observed were significantly different [32].

The 2D Cartesian model (26) generalizes the 1D model (23) in the same way as 3D model (10) generalizes the 2D polar model (16), as both these more common models can be produced by introducing the depth dimension and the additional equation for the oxygen concentration w. On the other hand, when reducing the mathematical model dimensionality the radial mass transport was assumed to be negligible due to the zero flux boundary conditions at the lateral surface ($\rho = R$). Since the dimensionless diffusion coefficient D_u and the chemotactic sensitivity χ are the main parameters controlling the mass transport in 1D model (23), the sensitivity of the spatiotemporal pattern formation to model parameters D_u and χ has to be investigated.

To investigate the influence of D_u and χ-parameters on the pattern formation the spatiotemporal patterns were simulated at different values of these parameters keeping values of the other parameters unchanged. Patterns simulated by using 1D model (23) are presented if Figs. 4–6. The patterns are compared between themselves as well as with the the corresponding patterns depicted in Fig. 2 obtained at $D_u = 0.1$ and $\chi = 8.3$ as defined in (35).

Figure 4 shows patterns for two values of the diffusion coefficient D_u: 0.2 and 0.3. The corresponding pattern obtained for a lower diffusivity ($D_u = 0.1$) of cells is depicted

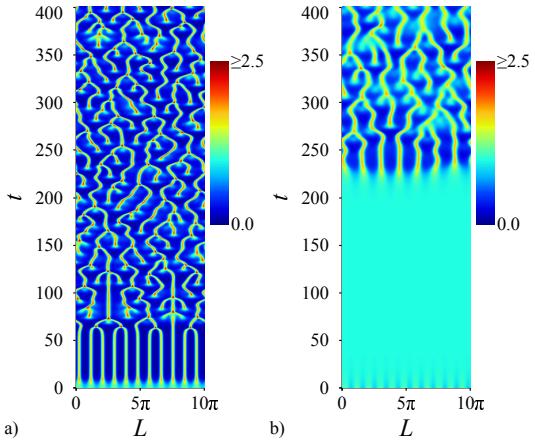

Fig. 4. Spatiotemporal plots of the dimensionless cell density u simulated by 1D model at two values of the dimensionless diffusion coefficient D_u: 0.2 (a) and 0.3 (b). Values of the other parameters are as defined in (35).

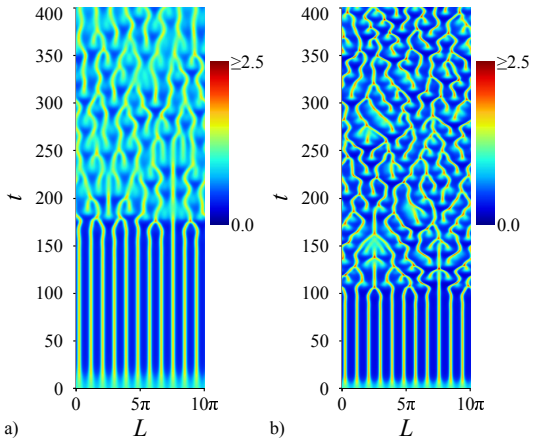

Fig. 5. Spatiotemporal plots of the dimensionless cell density u simulated by 1D model at two values of the chemotactic sensitivity χ: 5.8 (a) and 6.3 (b). Values of the other parameters are as defined in (35).

in Fig. 2a. It is noticeable that when increasing D_u-value, the spatiotemporal patterns seem to become thicker and a bit less prone to merge which makes them more similar to Fig. 2b and to those observed experimentally [40, 41, 42].

Similarly, when decreasing χ parameter value, patterns (Fig. 5) also tend to become thicker and a bit less prone to merge and in a similar way become more familiar to Fig. 2b. Spatiotemporal patters similar to that shown in Fig. 2b were also obtained at some other values of the parameters: $(D_u, \chi) = (0.15, 6.8)$ and $(D_u, \chi) = (0.09, 5.8)$ as shown in Fig. 6.

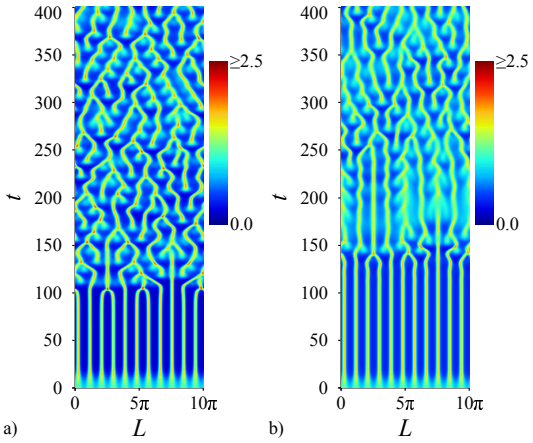

Fig. 6. Spatiotemporal plots of the dimensionless cell density u simulated by 1D model at different values of the model parameters: $D_u = 0.15, \chi = 6.8$ (a) and $D_u = 0.09, \chi = 5.8$ (b). Values of the other parameters are as defined in (35).

Figures 4–6 shows that the modelling error raised when reducing the model dimensionality can be at least partially compensated by adjusting values of D_u and/or χ-parameters. The compensation mechanism for 1D chemotaxis model, when an increase in one parameter can be compensated by decreasing or increasing another one, has been already investigated in detail [2, 10, 26]. Particularly, cell growth could compensate any loss of cells from one aggregate to a neighbour [26]. For three dimensional case the influence of the model parameters to the pattern formation and developing a model containing a minimal number of parameters and ensuring a qualitative analysis of bacterial pattern formation in a liquid medium is in progress.

5 Conclusions

We have shown that the Keller–Segel approach can be successfully used to describe the formation of bioluminescence patterns representing the self-organization of the bacteria in a rounded container (Figs. 1 and 3).

The 3D mathematical model (2)–(8) and the corresponding dimensionless model (10)–(15) of the bacterial self-organization in a rounded container as detected by bioluminescence imaging can be successfully used to simulate structures (Fig. 3) similar to the experimentally observed structures [41, 42] as well as to study the pattern formation in a colony of luminous *E. coli*.

Although the rounded container is best represented by the 3D model, due to the accumulation of luminous cells near the three phase contact line, the experimental spatiotemporal patterns of the bioluminescence can be qualitatively simulated also by using 1D and 2D models. Nevertheless, important differences in the shape of the patterns are

observed between the 1D, 2D and 3D cases when the same values of the model parameters are applied in the simulations (Fig. 2).

Very similar spatiotemporal patterns of the bioluminescence can be simulated using mathematical models of different dimensionality by adjusting values of the model parameters, particularly of the dimensionless diffusion coefficient and/or chemotactic sensitivity (Figs. 4-6).

References

1. M. Aida, T. Tsujikawa, M. Efendiev, A. Yagi, M. Mimura, Lower estimate of the attractor dimension for a chemotaxis growth system, *J. London Math. Soc.*, **74**(2):453–474, 2006.

2. R. Baronas, R. Šimkus, Modeling the bacterial self-organization in a circular container along the contact line as detected by bioluminescence imaging, *Nonlinear Anal. Model. Control*, **16**(3):270–282, 2011.

3. R. Baronas, Ž. Ledas, R. Šimkus, Computational modeling of self-organization in a liquid phase bacterial bioluminescent biosensor, in J. Eberhardsteiner et al. (Ed.), *Proceedings of the 6th European Congress on Computational Methods in Applied Sciences and Engineering (ECCOMAS 2012), Vienna, September 10–14, 2012*, Vienna University of Technology, Paper ID: 4815, 8 pp.

4. E. Ben-Jacob, I. Cohen, H. Levine, Cooperative self-organization of microorganisms, *Adv. Phys.*, **49**(4):395–554, 2000.

5. M.P. Brenner, L.S. Levitov, E.O. Budrene, Physical mechanisms for chemotactic pattern formation by bacteria, *Biophys. J.*, **74**(4):1677–1693, 1998.

6. E.O. Budrene, H.C. Berg, Dynamics of formation of symmetrical patterns by chemotactic bacteria, *Nature*, **376**(6535):49–53, 1995.

7. M.E. Cates, D. Marenduzzo, I. Pagonabarraga, J. Tailleur, Arrested phase separation in reproducing bacteria creates a generic route to pattern formation, *PNAS*, **107**(26):11715–11720, 2010.

8. A. Chertock, K. Fellner, A. Kurganov, A. Lorz, P.A. Markowich, Sinking, merging and stationary plumes in a coupled chemotaxis-fluid model: A high-resolution numerical approach, *J. Fluid Mech.*, **694**:155–190, 2012.

9. M.D. Egbert, X.E. Barandiaran, E.A. Di Paolo, A minimal model of metabolism-based chemotaxis, *PLoS Comput. Biol.*, **6**(12):e1001004, 2010.

10. S.-I. Ei, H. Izuhara, M. Mimura, Spatio-temporal oscillations in the Keller–Segel system with logistic growth, *Physica D*, **277**:1–21, 2014.

11. M. Eisenbach, *Chemotaxis*, Imperial College Press, London, 2004.

12. N.A. Hill, T.J. Pedley, Bioconvection, *Fluid Dyn. Res.*, **37**(1–2):1–20, 2005.

13. T. Hillen, K.J. Painter, A user's guide to pde models for chemotaxis, *J. Math. Biol.*, **58**(1–2):183–217, 2009.

14. T. Hillen, J. Zielinski, K.J. Painter, Merging-emerging systems can describe spatio-temporal patterning in a chemotaxis model, *Discret. Contin. Dyn. Syst. B*, **18**(10):2513–2536, 2013.

15. A.J. Hillesdon, T. J. Pedley, O. Kessler, The development of concentration gradients in a suspension of chemotactic bacteria, *Bull. Math. Bio.*, **57**:299–344, 1995.

16. D. Horstmann, From 1970 until present: The Keller–Segel model in chemotaxis and its consequences, *I. Jahresberichte DMV*, **105**(3):103–165, 2003.

17. R. Huzimura, T. Matsuyama, A mathematical model with a modified logistic approach for singly peaked population processes, *Theor. Popul. Biol.*, **56**(3):301–306, 1999.

18. P. Jorjani, S.S. Ozturk, Effects of cell density and temperature on oxygen consumption rate for different mammalian cell lines, *Biotechnol. Bioeng.*, **64**(3):349–356, 1999.

19. L.V. Kalachev, T.C. Kelly, M.J. O'Callaghan, A.V. Pokrovskii, A.V. Pokrovskiy, Analysis of threshold-type behaviour in mathematical models of the intrusion of a novel macroparasite in a host colony, *Math. Med. Biol.*, **28**(4):287–333, 2011.

20. K. Kawasaki, A. Mochizuki, M. Matsushita, T. Umeda, N. Shigesada, Modeling spatio-temporal patterns generaged by *Bacillus subtilis*, *J. Theor. Biol.*, **188**(2):177–185, 1997.

21. E.F. Keller, L.A. Segel, Model for chemotaxis, *J. Theor. Biol.*, **30**(2):225–234, 1971.

22. K. Kuto, K. Osaki, T. Sakurai, T. Tsujikawa, Spatial pattern formation in a chemotaxis-diffusion-growth model, *Physica D*, **241**(19):1629–1639, 2012.

23. P.K. Maini, M.R. Myerscough, K.H. Winters, J.D. Murray, Bifurcating spatially heterogeneous solutions in a chemotaxis model for biological pattern generation, *Bull. Math. Biol.*, **53**(5):701–719, 1991.

24. J.D. Murray, *Mathematical Biology: II. Spatial Models and Biomedical Applications*, 3rd ed., Springer, Berlin, 2003.

25. M.R. Myerscough, P.K. Maini, K.J. Painter, Pattern formation in a generalized chemotactic model, *Bull. Math. Biol.*, **60**(1):1–26, 1998.

26. K.J. Painter, T. Hillen, Spatio-temporal chaos in a chemotactic model, *Physica D*, **240**(4-5):363–375, 2011.

27. N. Perry, Experimental validation of a critical domain size in reaction-diffusion systems with *Escherichia coli* populations, *J. R. Soc. Interface*, **2**(4):379–387, 2005.

28. A. Rabner, E. Martinez, R. Pedhazur, T. Elad, S. Belkin, Y. Shacham, Mathematical modeling of a bioluminescent e. coli based biosensor, *Nonlinear Anal. Model. Control*, **14**(4):505–529, 2009.

29. P. Romanczuk, U. Erdmann, H. Engel, L. Schimansky-Geier, Beyond the Keller–Segel model. Microscopic modeling of bacterial colonies with chemotaxis, *Eur. Phys. J. Special Topics*, **157**(1):61–77, 2007.

30. A.A. Samarskii, *The Theory of Difference Schemes*, Marcel Dekker, New York, Basel, 2001.

31. H. Shoji, M. Nonomura, K. Yamada, Three-dimensional specific patterns based on the Keller–Segel model, *Forma*, **27**(1):19–23, 2012.

32. J. Stenhammar, D. Marenduzzo, R.J. Allen, M.E. Cates, Phase behaviour of active Brownian particles: The role of dimensionality, *Soft Matter*, **10**(10):1489–1499, 2014.

33. M.J. Tindall, P.K. Maini, S.L. Porter, J.P. Armitage, Overview of mathematical approaches used to model bacterial chemotaxis II: Bacterial populations, *Bull. Math. Biol.*, **70**(6):1570–1607, 2008.

34. I. Tuval, L. Cisneros, C. Dombrowski, C.W. Wolgemuth, J. Kessler, R.E. Goldstein, Bacterial swimming and oxygen transport near contact lines, *Proc. Natl. Acad. Sci. USA*, **102**(7):2277–2282, 2005.

35. R. Tyson, S.R. Lubkin, J.D. Murray, A minimal mechanism for bacterial pattern formation, *Proc. R. Soc. Lond. B*, **266**(1416):299–304, 1999.

36. R. Tyson, S.R. Lubkin, J.D. Murray, Model and analysis of chemotactic bacterial patterns in a liquid medium, *J. Math. Biol.*, **38**(4):359–375, 1999.

37. R. Tyson, L.G. Stern, R.J. LeVeque, Fractional step methods applied to a chemotaxis model, *J. Math. Biol.*, **41**(5):455–475, 2000.

38. R. Čiegis, A. Bugajev, Numerical approximation of one model of bacterial self-organization, *Nonlinear Anal. Model. Control*, **17**(3):253–270, 2012.

39. R. Šimkus, Bioluminescent monitoring of turbulent bioconvection, *Luminescence*, **21**(2):77–80, 2006.

40. R. Šimkus, R. Baronas, Metabolic self-organization of bioluminescent *Escherichia coli*, *Luminescence*, **26**(6):716–721, 2011.

41. R. Šimkus, R. Baronas, Ž. Ledas, A multi-cellular network of metabolically active *E. coli* as a weak gel of living janus particles, *Soft Matter*, **9**(17):4489–4500, 2013.

42. R. Šimkus, V. Kirejev, R. Meškienė, R. Meškys, Torus generated by *Escherichia coli*, *Exp. Fluids*, **46**(2):365–369, 2009.

43. M. Winkler, Boundedness in the higher-dimensional parabolic-parabolic chemotaxis system with logistic source, *Comm. PDEs*, **35**(8):1516–1537, 2010.

44. M.P. Zorzano, D. Hochberg, M.T. Cuevas, J.M. Gomez-Gomez, Reaction-diffusion model for pattern formation in *E. coli* swarming colonies with slime, *Phys. Rev. E*, **71**(3), 031908, 6 pp., 2005.